Supporting Information:

Heme/Copper Assembly Mediated Nitrite and Nitric Oxide Interconversion

Shabnam Hematian, Maxime A. Siegler and Kenneth D. Karlin*

Department of Chemistry, Johns Hopkins University, Baltimore, MD, 21218 USA

Contents:

1. Materials and Methods.

Unless otherwise stated all solvents and chemicals used were of commercially available analytical grade. Dichloromethane (CH_2Cl_2), diethyl ether (Et_2O), and methanol (MeOH) were used after passing them through a 60 cm long column of activated alumina (Innovative Technologies, Inc.) under argon. Tetrahydrofuran (THF) and 2-Methyltetrahydrofuran (MeTHF) (Sigma, 673277, inhibitor free) were purified and dried by distillation from sodium/benzophenone ketyl under argon. Pentane and acetonitrile (MeCN) were dried by distillation over calcium hydride and acetone was freshly distilled from Drierite (anhydrous calcium sulfate) under argon prior to use. Dioxygen was dried by passing through a short column of supported P_4O_{10} (Aquasorb, Mallinkrodt). Nitrogen monoxide (NO) gas was obtained from Matheson Gases. Following methods previously described in the literature,[1] nitric oxide was purified by passage through a series of two KOH columns and finally distilled at 195 K and then collected in an evacuated Schlenk flask (typically 50 mL) fitted with a septum. Addition of $NO_{(g)}$ to metal complex solutions was effected by transfer via a three-way long syringe needle. Preparation and handling of air sensitive compounds were performed under an argon atmosphere using standard Schlenk techniques or in an MBraun Labmaster 130 inert atmosphere (<1 ppm O_2, <1 ppm H_2O) drybox filled with nitrogen. Deoxygenation of solvents was effected by either repeated freeze/pump/thaw cycles or bubbling with argon for 45 - 60 min.

Elemental analyses were performed by Columbia Analytical Services (Tucson, AZ). UV-vis spectra were recorded on a Cary-50 Bio spectrophotometer equipped with a fiber optic coupler (Varian). Spectrophotometer cells used were made by Quark Glass with column and pressure/vacuum side stopcock and 1 cm path length. ^{1}H-NMR spectra were acquired using a Bruker 400 MHz spectrometer. Chemical shifts were reported as δ values relative to an internal standard (Me_4Si) and the residual solvent proton peak. Electron paramagnetic resonance (EPR) spectra were recorded on a Bruker EMX spectrometer controlled with a Bruker ER 041 X G microwave bridge operating at X-band (~9.4 GHz). Infrared spectra (IR) were obtained using a Thermo Scientific Nicolet Nexus 670 FT-IR spectrophotometer.

X-ray diffraction was performed at the X-ray diffraction facility at the Johns Hopkins University. All reflection intensities were measured at 110(2) K using a KM4/Xcalibur (detector: Sapphire3) with enhance graphite-monochromated Mo *K*α radiation (λ = 0.71073 Å) under the program CrysAlisPro (Versions 1.171.33.31 or 1.171.35.11, Agilent Technologies, 2011). The program CrysAlisPro (Versions 1.171.33.31 or 1.171.35.11, Agilent Technologies, 2011) was used to refine the cell dimensions. Data reduction was done using the program CrysAlisPro (Versions 1.171.33.31 or 1.171.35.11, Agilent Technologies, 2011). The structure was solved with the program SHELXS-97[2] and was refined on F^2 with SHELXL-97.[2] Analytical numeric absorption corrections based on a multifaceted crystal model were applied using CrysAlisPro (Versions 1.171.33.31 or 1.171.35.11, Agilent Technologies, 2011). The temperature of the data collection was controlled using the system Cryojet (manufactured by Oxford Instruments). The H atoms were placed at calculated positions using the instructions AFIX 23 or AFIX 43 with isotropic displacement parameters having values 1.2 times *U*eq of the attached C atoms. The structure of $[(tmpa)Cu^{II}(Cl)][B(C_6F_5)_4]$ is ordered. The structure of $[(tmpa)Cu^{II}(NO_2)][B(C_6F_5)_4]$ is found to be mostly ordered; the nitrite ion is disordered over two orientations. The occupancy factor of the major orientation refines to 0.875(5). $[(tmpa)Cu^{II}(Cl)][B(C_6F_5)_4]$, Fw = 1068.40, turquoise blue block, 0.49 × 0.20 × 0.16 mm^3, orthorhombic, *Pbca* (no. 61), *a* = 13.08228(15), *b* = 23.1771(3), *c* =

26.3615(3) Å, V = 7993.05(17) Å^3, Z = 8, D_x = 1.776 g cm^{-3}, μ = 0.747 mm^{-1}, abs. corr. range: 0.78–0.90. 50400 Reflections were measured up to a resolution of (sin $\theta/\lambda)_{max}$ = 0.62 Å^{-1}. 7840 Reflections were unique (R_{int} = 0.055), of which 5584 were observed [$I > 2\sigma(I)$]. 622 Parameters were refined. $R1/wR2$ [$I > 2\sigma(I)$]: 0.0305/0.0665. $R1/wR2$ [all refl.]: 0.0525/0.0699. S = 0.932. Residual electron density found between −0.58 and 0.34 eÅ^{-3}. [(tmpa)Cu^{II}(NO$_2$)][B(C$_6$F$_5$)$_4$], Fw = 1078.96, green block, 0.67 × 0.37 × 0.21 mm^3, orthorhombic, *Pbca* (no. 61), a = 13.3059(2), b = 22.9396(5), c = 26.0492(7) Å, V = 7951.1(3) Å^3, Z = 8, D_x = 1.803 g cm^{-3}, μ = 0.692 mm^{-1}, abs. corr. range: 0.711–0.894. 25595 Reflections were measured up to a resolution of (sin $\theta/\lambda)_{max}$ = 0.62 Å^{-1}. 8030 Reflections were unique (R_{int} = 0.0356), of which 6640 were observed [$I > 2\sigma(I)$]. 659 Parameters were refined using 63 restraints. $R1/wR2$ [$I > 2\sigma(I)$]: 0.0317/0.0784. $R1/wR2$ [all refl.]: 0.0428/0.0833. S = 1.034. Residual electron density found between −0.58 and 0.39 e Å^{-3}.[2]

A capillary electrophoresis (CE) instrument from Beckman Coulter (P/ACE MDQ, Fullerton, CA) equipped with diode-array UV-vis detector was used to measure nitrite concentrations. Bare fused silica capillary (Polymicro Technologies, Phoenix, AZ) with 75 μm ID × 60 cm total length was used for separation. Capillary and sample board temperature was thermostatted to 25^{o}C during operation. Between experiments, the capillary was sequentially rinsed by flushing distilled, deionized water (DDW) for 0.5 min, 0.1 M NaOH for 1 min, DDW again for 1 min, and capillary electrolyte for 2.5 min. Samples were introduced into the capillary by hydrostatic injection using a pressure of 0.5 psi for 10 s at an applied negative potential of 25 kV, and UV detection at 220 nm. The background electrolyte consisted of 25 mM sodium phosphate (pH 7.0) and 0.5 mM tetradecyltrimethylammonium chloride (TTAC) electroosmotic flow modifier. Cyclic voltammetic measurements were undertaken in acetone solvent under argon at room temperature using a BAS 100B/W electrochemical analyzer with a glassy carbon working electrode and a platinum wire auxiliary electrode. Potentials were recorded versus an Ag/AgNO$_3$ reference electrode. Scans were run at 100 mV/s using ~0.1 M tetrabutylammonium hexafluorophosphate

($(Bu)_4N(PF_6)$) as the supporting electrolyte. The voltammograms are plotted versus the $Fe(Cp)_2^{+/0}$ potential which was measured as an external standard under the same elctrochemical cell conditions.

Tris(2-pyridylmethyl)amine (tmpa),[3] $[(tmpa)Cu^{II}(MeCN)](ClO_4)_2$,[4] $(F_8)Fe^{III}(OH)$,[5] $[(F_8)Fe^{III}]SbF_6$,[6] $(F_8)Fe^{II}$,[7] and $[H(C_2H_5OC_2H_5)_2][B(C_6F_5)_4]$ (HBArF)[8] were synthesized and characterized following methods previously described in the literature. $[(F_8)Fe^{III}\text{-}O\text{-}Cu^{II}(tmpa)][B(C_6F_5)_4]$[9] was prepared by bubbling dry dioxygen through the 1:1 solution of $(F_8)Fe^{II}$ and $[(tmpa)Cu^{I}(MeCN)][B(C_6F_5)_4]$ in MeTHF for 2 min and the mixture was allowed to stir for 2 h at RT. The solvent was then removed under vacuum and solid was further dried under vacuum for additional 6 h. $[(F_8)Fe^{III}\text{-}(OH)\text{-}Cu^{II}(tmpa)][B(C_6F_5)_4]_2$ [8] was synthesized by addition of 1 equiv HBArF to the $[(F_8)Fe^{III}\text{-}O\text{-}Cu^{II}(tmpa)][B(C_6F_5)_4]$ in MeTHF and solution was stirred for 10 min and then dried under vacuum for several hours.

2. Synthesis of $[(tmpa)Cu^{II}(Cl)][B(C_6F_5)_4]$

$CuCl_2.2H_2O$ (171 mg, 1.00 mmol) and tmpa (290 mg, 1.00 mmol) were dissolved in 10 mL of MeCN followed by addition of five drops of water to form a clear blue solution. After stirring for 5 min, $K[B(C_6F_5)_4]$ (718 mg, 1.00 mmol) was added to the reaction mixture, causing a white precipitate to form. The reaction mixture was concentrated to dryness under reduced pressure leaving a crude residue, which was redissolved in diethyl ether, filtered, giving a turquoise blue solution. The solvent was then removed under reduced pressure and recrystallization of the resulting soild from hot MeOH/water afforded turquoise blue good-quality crystals suitable for X-ray structure determination. After vacuum-drying the crystals weighed 887 mg (83% yield). Anal. Calcd for $C_{42}H_{18}BClCuF_{20}N_4$: C, 47.22; H, 1.70; N, 5.24. Found: C, 47.43; H, 2.11; N, 5.03. UV-vis spectrum (**Figure S1**) in acetone (λ_{max}, nm (ε_{max}, $M^{-1}cm^{-1}$)): 961 (205); 745 (90, sh). EPR spectrum (**Figure S2**): X-band spectrometer (ν = 9.428 GHz) in MeTHF at 21 K: $g_{\|} \approx 2.004$, $A_{\|} \approx 70$ G, $g_{\perp} = 2.190$, $A_{\perp} = 96$ G. These data are typical for trigonal bipyramidal copper(II) structures.[10]

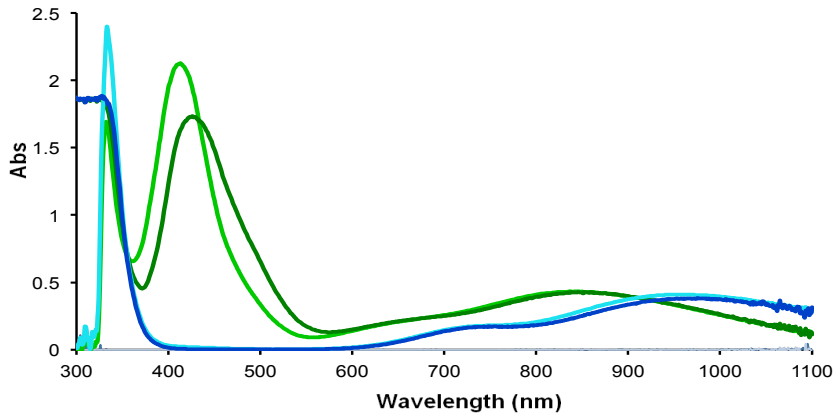

Figure S1. UV-vis spectra of $[(tmpa)Cu^{II}(Cl)][B(C_6F_5)_4]$ in acetone (**light blue**) in MeTHF (**dark blue**) and $[(tmpa)Cu^{II}(NO_2)][B(C_6F_5)_4]$ in acetone (**light green,** $\lambda_{max} = 413$ nm) in MeTHF (**dark green,** $\lambda_{max} = 427$ nm) (2mM).

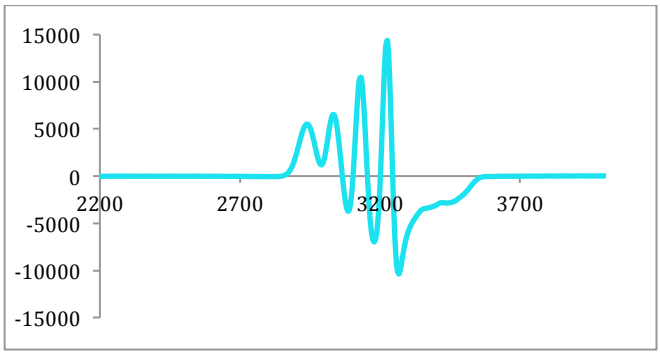

Figure S2. EPR spectrum of $[(tmpa)Cu^{II}(Cl)][B(C_6F_5)_4]$ (2mM) in MeTHF at 20 K.

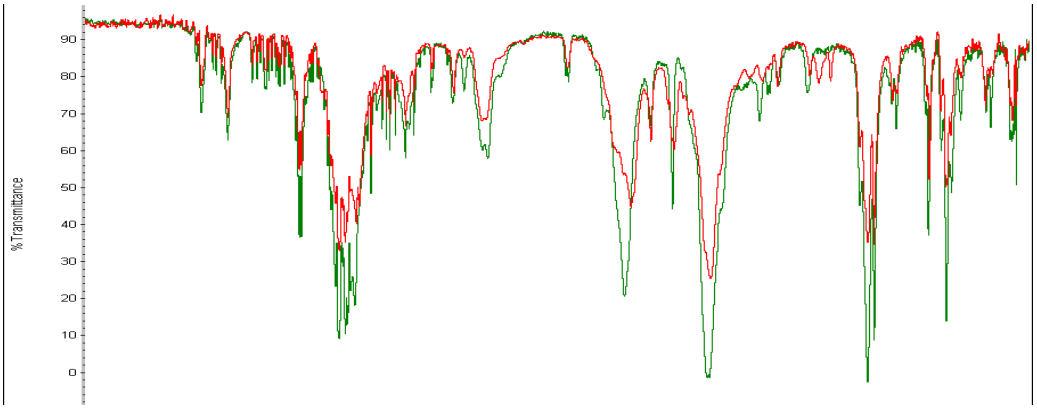

Figure S3. IR spectra (solid) comparison between the two Cu^{II} complexes: $[(tmpa)Cu^{II}(Cl)][B(C_6F_5)_4]$ (**green**) $[(tmpa)Cu^{II}(NO_2)][B(C_6F_5)_4]$ (**red**).

3. Crystal structure of $[(tmpa)Cu^{II}(Cl)][B(C_6F_5)_4]$

A displacement ellipsoid plot (50% probability level) of the cationic fragment, $[(tmpa)Cu^{II}(Cl)]^+$, is presented in **Figure S4**. The structure is five-coordinate, with ligation to the three pyridyl and single aliphatic nitrogen atoms of the ligand (N(1), N(2), N(3) and N(4)), accompanied by an interaction of the cupric ion with the chloride ion (Cl1). Selected bond distances and angles are given in the Figure S4 caption. The geometry about the copper atom is trigonal bipyramidal ($\tau = 1$)[11] with the amine nitrogen N(2) and chloride ion occupying the axial positions and the pyridyl nitrogens (N(1), N(3), N(4)) in the trigonal plane.

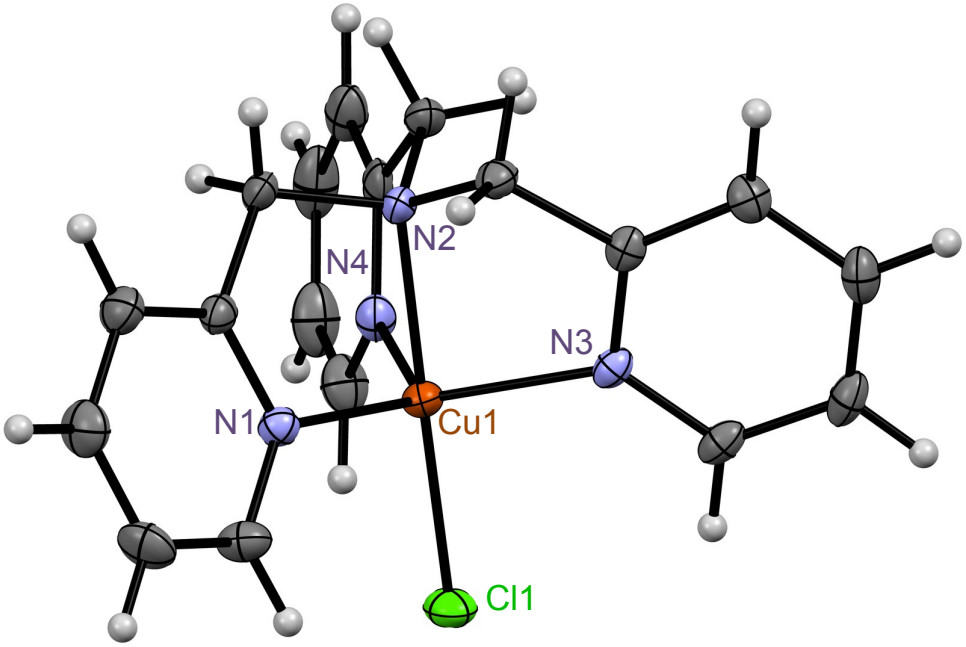

Figure S4. Displacement ellipsoid plot (50% probability level) of $[(tmpa)Cu^{II}(Cl)]^+$, showing the atom-labeling scheme. Relevant bond lengths (Å) and angles (deg): Cu-N(1), 2.074 (2); Cu-N(2), 2.045 (1); Cu-N(3), 2.078 (2); Cu-N(4), 2.052 (6); Cu-Cl(1), 2.221 (9); N(2)-Cu-N(4), 81.3 (8); N(2)-Cu-N(1), 81.0 (3); N(2)-Cu-N(3), 81.7 (1); N(4)-Cu-N(1), 121.5 (1); N(4)-Cu-N(3), 118.3 (7); N(1)-Cu-N(3), 113.4 (7); N(2)-Cu-C1(1), 178.3 (2); N(4)-Cu-Cl(1), 97.2 (1); N(1)-Cu-C1(1), 100.5 (1); N(3)-Cu-C1(1), 98.2 (1).

4. Synthesis of [(tmpa)$Cu^{II}(NO_2)$][$B(C_6F_5)_4$]

Silver nitrite (77 mg, 0.50 mmol) was added to [(tmpa)Cu^{II}(Cl)][$B(C_6F_5)_4$] (534 mg, 0.50 mmol) in 10 mL of methanol resulting a green solution and precipitation of AgCl. The reaction mixture was sonicated for 5 min, and followed by filtration. Then, the filtrate was heated and gently recrystallized by slow addition of water yielding 421 mg (78%) of green crystals. Anal. Calcd for $C_{42}H_{18}BCuF_{20}N_5O_2$: C, 46.75; H, 1.68; N, 6.49. Found: C, 46.93; H, 2.25; N, 6.21. UV-vis spectrum (**Figure S1**) in acetone (λ_{max}, nm (ε_{max}, $M^{-1}cm^{-1}$)): 843 (216); 413 (1156) (A small bathochromic shift was observed for the latter spectral band in MeTHF (λ_{max} = 427 nm)). EPR spectrum (**Figure S5**): X-band spectrometer (ν = 9.426 GHz) in MeTHF at 21 K: $g_{\|}$ = 1.992, $A_{\|}$ = 84 G, $g_{\perp}$ = 2.200, $A_{\perp}$ = 102 G. FT-IR spectrum (solid) (**Figure S3**): ν(N=O) 1435 cm^{-1}, ν(N–O) 1076 cm^{-1}, and $\delta(NO_2)$ 813 and 829 cm^{-1}. The infrared spectrum of [(tmpa)$Cu^{II}(NO_2)$][$B(C_6F_5)_4$] is mainly characterized by the nitrite ligand vibrations. Although nitrite vibrations can only be assigned certainly by isotope labeling, they are tentatively attributed here through the spectra differences between [(tmpa)$Cu^{II}(NO_2)$][$B(C_6F_5)_4$] and its chloride precursor.

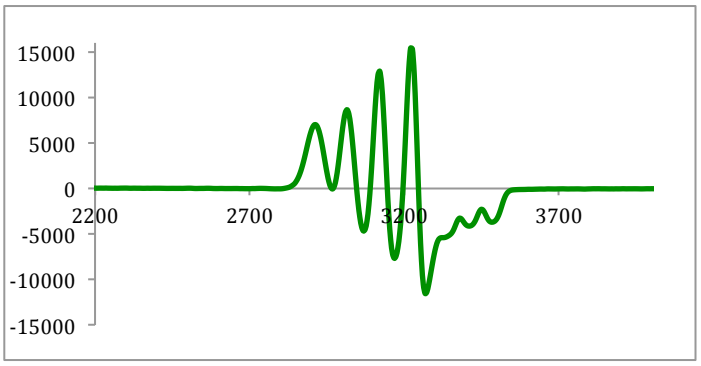

Figure S5. EPR spectrum of [(tmpa)$Cu^{II}(NO_2)$][$B(C_6F_5)_4$] (2mM) in MeTHF at 20 K.

5. Crystal structure of [(tmpa)$Cu^{II}(NO_2)$][$B(C_6F_5)_4$]

The structure consists of isolated [(tmpa)$Cu^{II}(NO_2)]^+$ cations and $[B(C_6F_5)_4]^-$ counter anions. The copper centers are penta-coordinated by the N donor atoms of tris(2-pyridylmethyl)amine ligand, and O(1) of a

monodentate nitrito ligand. The structure of $[(tmpa)Cu^{II}(NO_2)]^+$ is, therefore, approximated by a trigonal bipyramidal geometry ($\tau = 0.9$), as shown by the data in **Figure S6**.

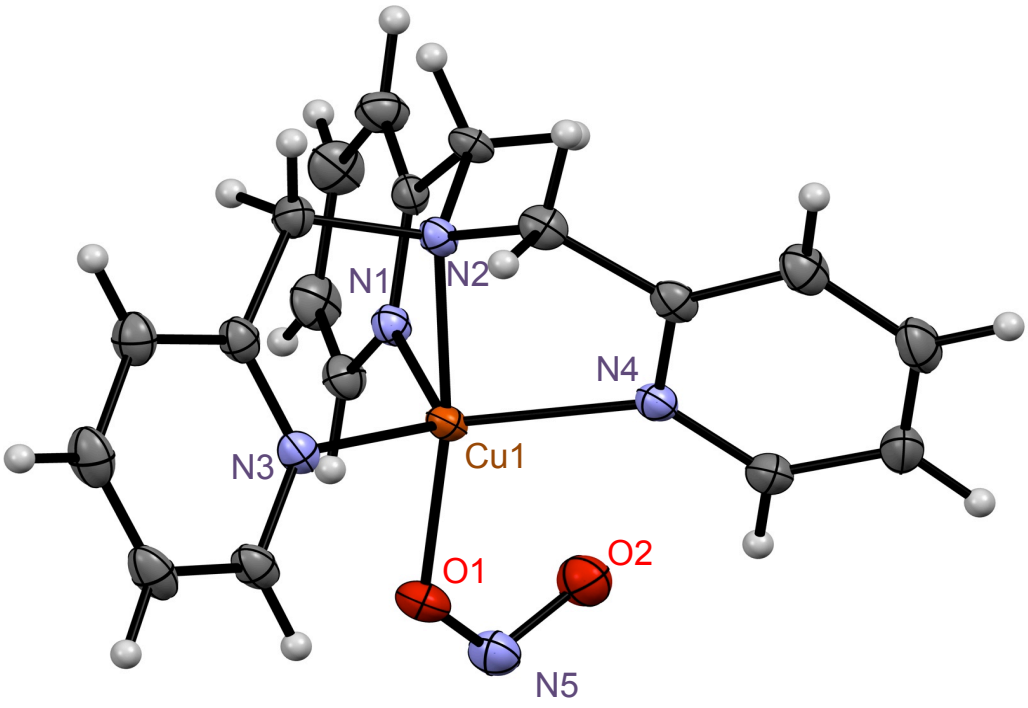

Figure S6. Displacement ellipsoid plot (50% probability level) of $[(tmpa)Cu^{II}(NO_2)]^+$, showing the atom-labeling scheme. The disorder observed for the nitrite ligand is not shown for the sake of clarity. Relevant bond lengths (Å) and angles (deg): Cu-N(1), 2.058 (2); Cu-N(2), 2.039 (9); Cu-N(3), 2.063 (5); Cu-N(4), 2.100 (7); Cu-O(1), 1.930 (9); O(1)-Cu-N(2), 170.6 (7); O(l)-Cu-N(1), 99.2 (0); N(2)-Cu-N(1), 81.3 (7); O(l)-Cu-N(3), 90.6 (9); N(2)-Cu-N(3), 81.0 (5); N(1)-Cu-N(3), 119.6 (6); O(1)-Cu-N(4), 107.3 (0); N(2)-Cu-N(4), 80.5 (2); N(1)-Cu-N(4), 115.9 (6); N(3)-Cu-N(4), 117.1 (5).

6. Synthesis of $[(tmpa)Cu^{I}(MeCN)][B(C_6F_5)_4]$

This synthesis followed a procedure similar to that reported earlier for a number of cuprous pyridyl-alkylamine compounds.[3,12] In a 100 ml Schlenk flask located in the drybox, 625 mg (0.69 mmol) of $[Cu^{I}(MeCN)_4][B(C_6F_5)_4]$[13] was dissolved in 7 ml THF. 200 mg (0.69 mmol) of tmpa ligand dissolved in approximately 3 ml of THF was added to the copper solution, resulting in an immediate color change

from colorless to red-orange. This solution was allowed to stir for 25 min followed by addition of 60 ml of deoxygenated pentane to the solution resulting precipitation. The supernatant was decanted and the compound obtained was recrystallized from THF/Pentane. The precipitate formed was dried under vacuum to afford 642 mg of a bright yellow-orange solid. (87% yield). ^{1}H-NMR (CD_3CN): δ 8.95 (br, 3H), 7.83 (m, 3H), 7.49 (br, 6H), 4.30 (vbr, 6H), 2.02 (s, 3H, CH_3CN).

7. Reaction of $2F_8Fe^{II}$ with $[(tmpa)Cu^{II}(NO_2)][B(C_6F_5)_4]$

In the drybox, F_8Fe^{II} (10.0 mg, 0.012 mmol) was dissolved in 50 mL acetone in a 100 mL Schlenk flask equipped with a magnetic stir bar. Then $[(tmpa)Cu^{II}(NO_2)][B(C_6F_5)_4]$ (6.6 mg, 0.006 mmol) was added to the solution and after stirring for 1 h, the solvent was removed to yield a brown solid. During the reaction, 305 μL aliquots were withdrawn by syringe every 10 min, diluted with acetone to 5.0 mL, and a UV-vis spectrum was recorded (**Figure S7**). The formation of 1:1 mixture of the $(F_8)Fe^{II}(NO)$ and the μ-oxo complex $[(F_8)Fe^{II}\text{-}O\text{-}Cu^{II}(tmpa)]^+$ was observed based on UV-vis spectrum{λ_{max} = 399 and 435 (Soret), 555 nm}; these spectral parameters matched those of previous reports for these products. The EPR spectrum of the product mixture (**Figure S8**) gave signals for $(F_8)Fe^{II}(NO)$ which has a distinctive three-line hyperfine splitting and was consistent with the presence of a 1:1 mixture of $(F_8)Fe^{II}(NO)$ and $[(F_8)Fe^{III}\text{-}O\text{-}Cu^{II}(tmpa)]^+$; the latter is an EPR-silent species. EPR quantification in acetone at 20 K, employing authentic $[(tmpa)Cu^{II}(MeCN)](ClO_4)_2$ and $(F_8)Fe^{III}(OH)$ separately revealed the presence of trace amounts (< 5%) of free Cu^{II} and Fe^{III} species suggesting that majority of Cu^{II} and Fe^{III} ions were converted to the μ-oxo complex, i.e. one equiv Fe^{III} was produced corresponding to one equiv nitrite reduced. In addition, the IR spectrum of the solid product (**Figure S9**) displayed a N-O stretching frequency at 1688 cm^{-1} due to formation of $(F_8)Fe^{II}(NO)$. Similar reaction products were obtained when instead $(Bu)_4N(NO_2)$ as nitrite source was used to carry out the reaction. In this reaction, 1 equiv tetrabutylammonium nitrite ($(Bu)_4N(NO_2)$) was added to the solution of $[(tmpa)Cu^{II}(MeCN)](ClO_4)_2$ in acetone and an immediate color change from blue to green was observed upon addition indicating rapid

coordination of nitrite to Cu^{II} ion. The resulting green solution was then added to the solution of 2 equiv F_8Fe^{II} in acetone followed by stirring for 1 h. The formation of the similar 1:1 product mixture of $(F_8)Fe^{II}(NO)$ and $[(F_8)Fe^{III}\text{-}O\text{-}Cu^{II}(tmpa)]^+$ was confirmed by UV-vis, EPR, and IR spectroscopies.

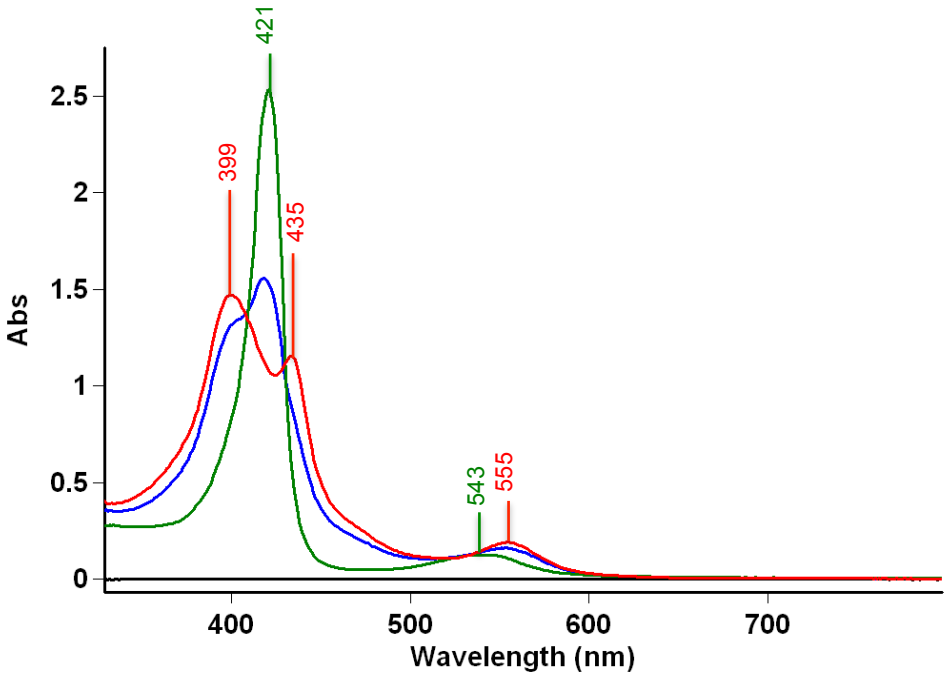

Figure S7. UV-vis spectra of F_8Fe^{II} (10 μM) (green, λ_{max} = 421 (Soret), 543 nm) and reaction solution of F_8Fe^{II} and ½[(tmpa)$Cu^{II}(NO_2)$][$B(C_6F_5)_4$] after stirring for 10 min (15 μM) (blue) and 1 h (15 μM) (red, λ_{max} = 399, 435 (Soret), 555 nm) in acetone at RT.

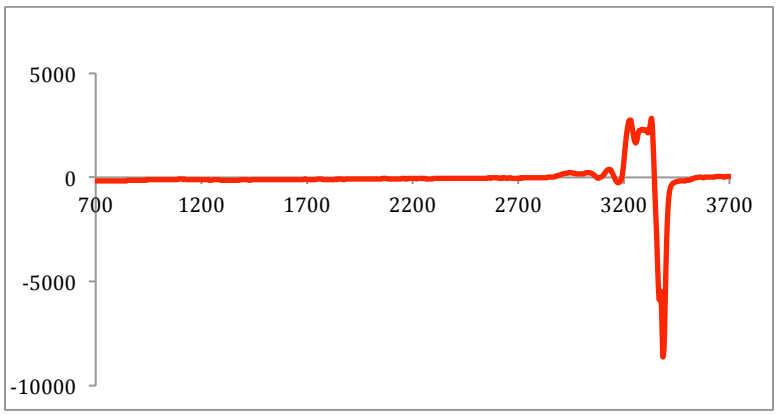

Figure S8. EPR spectrum of the reaction solution of F_8Fe^{II} and ½[(tmpa)$Cu^{II}(NO_2)$][$B(C_6F_5)_4$] (2mM) in acetone at 20 K.

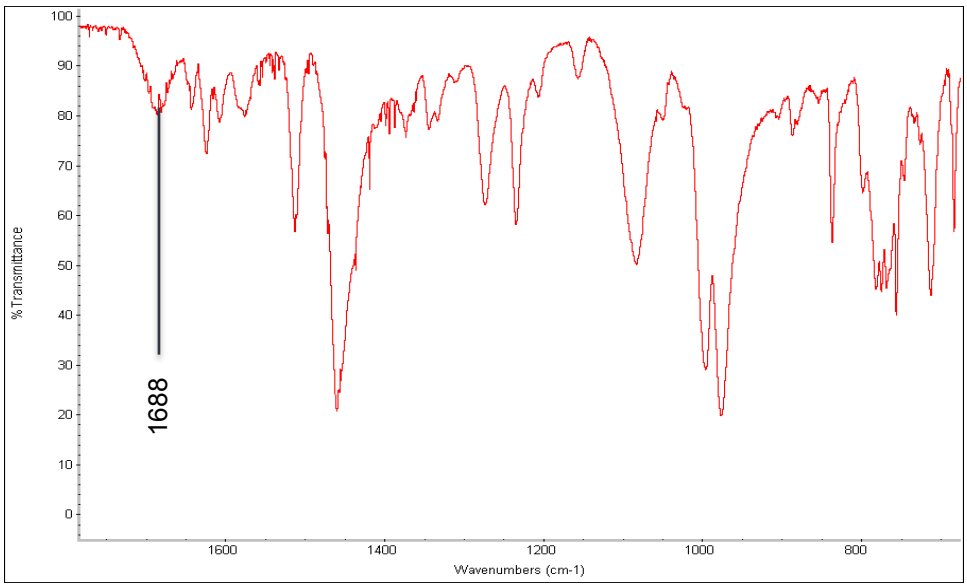

Figure S9. IR spectrum of the solid product of the reaction of F_8Fe^{II} and ½[(tmpa)$Cu^{II}(NO_2)$][$B(C_6F_5)_4$].

8. Reaction of $F_8Fe^{III}SbF_6$ and Nitrite with [(tmpa)Cu^{I}(MeCN)][$B(C_6F_5)_4$]

$(F_8)Fe^{III}(SbF_6)$•2THF (14.7 mg, 0.012 mmol) was dissolved in 50 mL deoxygenated acetone in a 100 mL Schlenk flask equipped with a magnetic stir bar. $(Bu)_4N(NO_2)$ (3.6 mg, 0.012 mmol) was added to the solution resulting in a large UV-vis change assigned to the formation of $(F_8)Fe^{III}(NO_2)$ {λ_{max} = 405 (Soret), 567 nm} **(Figure S10)**. After stirring for 10 min, reduced complex [(tmpa)Cu^{I}(MeCN)][$B(C_6F_5)_4$] (13.2 mg, 0.012 mmol) was added to the solution and stirred for several hours. UV-vis spectra showed no significant change even after stirring for days. In order to prepare UV-vis samples, 305 µL aliquots were withdrawn by syringe and diluted with acetone to 5.0 mL (15 µM). UV-vis spectra showed no significant change even after stirring for days indicating no nitrite reduction proceeded **(Figure S10)**.

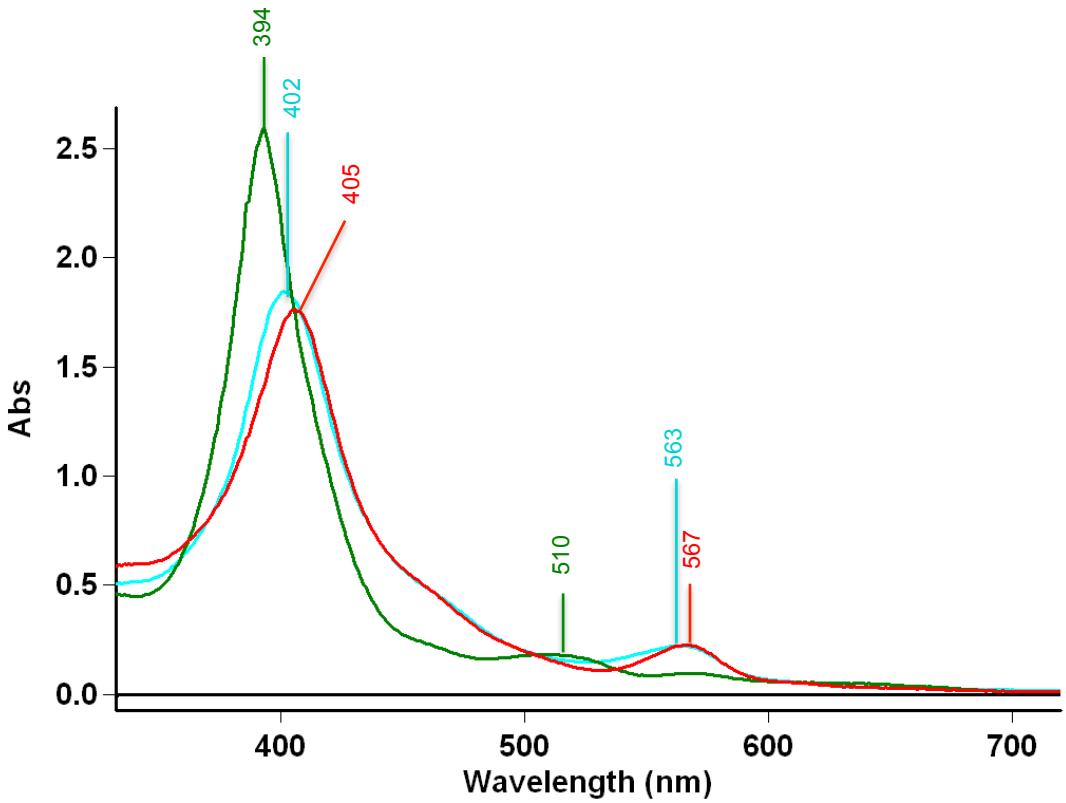

Figure S10. UV-vis spectra of $(F_8)Fe^{III}(SbF_6)$ (green, λ_{max} = 394 (Soret), 510 nm) and $(F_8)Fe^{III}(NO_2)$ obtained by addition of 1 equiv $(Bu)_4N(NO_2)$ to solution of $(F_8)Fe^{III}(SbF_6)$ (red, λ_{max} = 405 (Soret), 567 nm) followed by addition of 1 equiv $[(tmpa)Cu^{I}(MeCN)][B(C_6F_5)_4]$ (blue, λ_{max} = 402 (Soret), 563 nm) 15 μM in acetone at RT.

9. Reaction of F_8Fe^{II} with Nitrite

In the drybox, to a 25 mL acetone solution of F_8Fe^{II} (10.0 mg, 0.012 mmol), $(Bu)_4N(NO_2)$ (3.6 mg, 0.012 mmol) was added. The mixture was stirred for several hours, without any significant color or UV-vis absorbance changes (**Figure S11**) indicating that nitrite reacts only very slowly with $(F_8)Fe^{II}$ in the absence of Cu^{II} as a Lewis Acid.

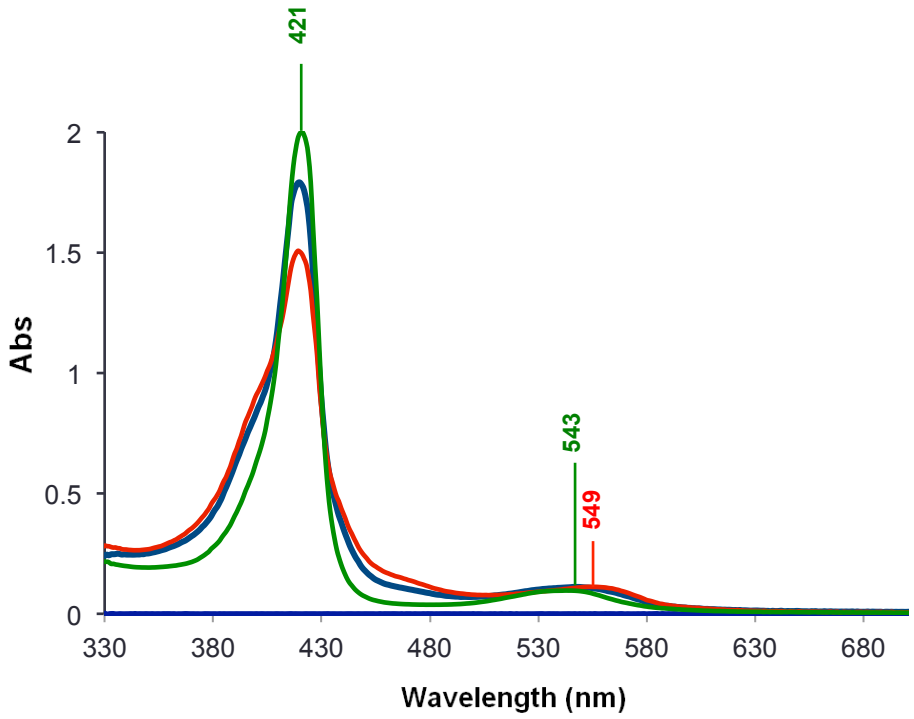

Figure S11. UV-vis spectra of F_8Fe^{II} (green, λ_{max} = 421 (Soret), 543 nm) and the reaction solution of F_8Fe^{II} and 1 equiv of $(Bu)_4N(NO_2)$ after stirring for 1 h (blue) for 5 h (red, λ_{max} = 421 (Soret), 549 nm) 10 μM in acetone at RT.

10. Reaction of [(tmpa)Cu^{I}(MeCN)][B(C_6F_5)$_4$] with Nitrite

In the drybox, to a 25 mL acetone solution of [(tmpa)Cu^{I}(MeCN)][B(C_6F_5)$_4$] (13.2 mg, 0.012 mmol), $(Bu)_4N(NO_2)$ (3.6 mg, 0.012 mmol) was added and the reaction mixture was allowed to stir for 2 days, with the color turning from bright yellow to yellow probably caused by generation of N-bound nitro-Cu^{I} complex. UV-vis spectra showed no absorbance in the 500-1100 nm range (**Figure S12**), and along with an EPR silent spectrum (acetone, 20 K), no occurrence of a redox reaction is indicated.

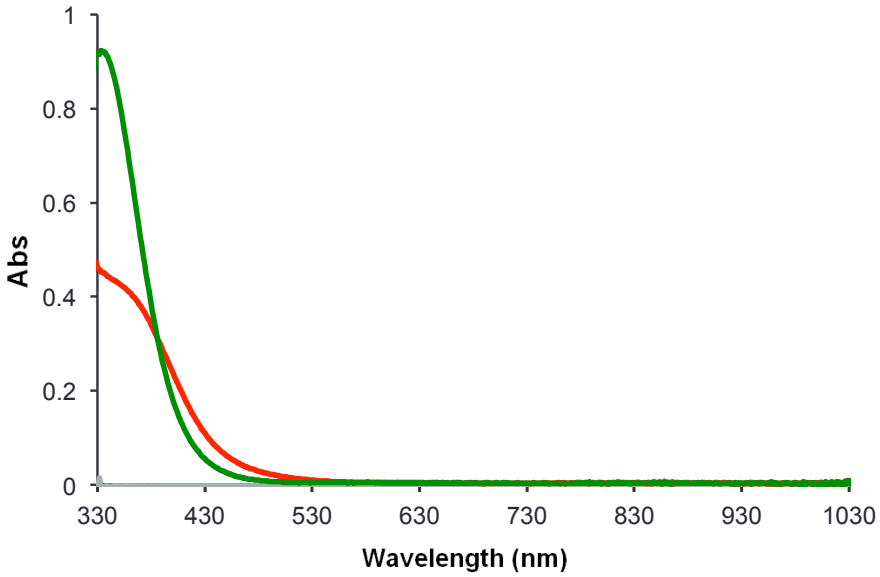

Figure S12. UV-vis spectra of [(tmpa)Cu^{I}(MeCN)][$B(C_6F_5)_4$] (green) and the reaction solution of [(tmpa)Cu^{I}(MeCN)][$B(C_6F_5)_4$] and 1 equiv of $(Bu)_4N(NO_2)$ after stirring for 2 days (red) in acetone at RT.

11. Reaction of F_8Fe^{II} and [(tmpa)Cu^{I}(MeCN)][$B(C_6F_5)_4$] with Nitrite

To a 25 mL acetone solution of F_8Fe^{II} (10.0 mg, 0.012 mmol), [(tmpa)Cu^{I}(MeCN)][$B(C_6F_5)_4$] (13.2 mg, 0.012 mmol) was added. The solution was stirred for 10 min, and then $(Bu)_4N(NO_2)$ (7.1 mg, 0.024 mmol) was introduced. A UV-vis spectrum was recorded after stirring for several hours and no significant absorbance change was observed (**Figure S13**). There was no detectable redox reaction occurring between nitrite and fully reduced complexes at RT under anaerobic conditions even after several hours, based on the UV-vis spectroscopic monitoring.

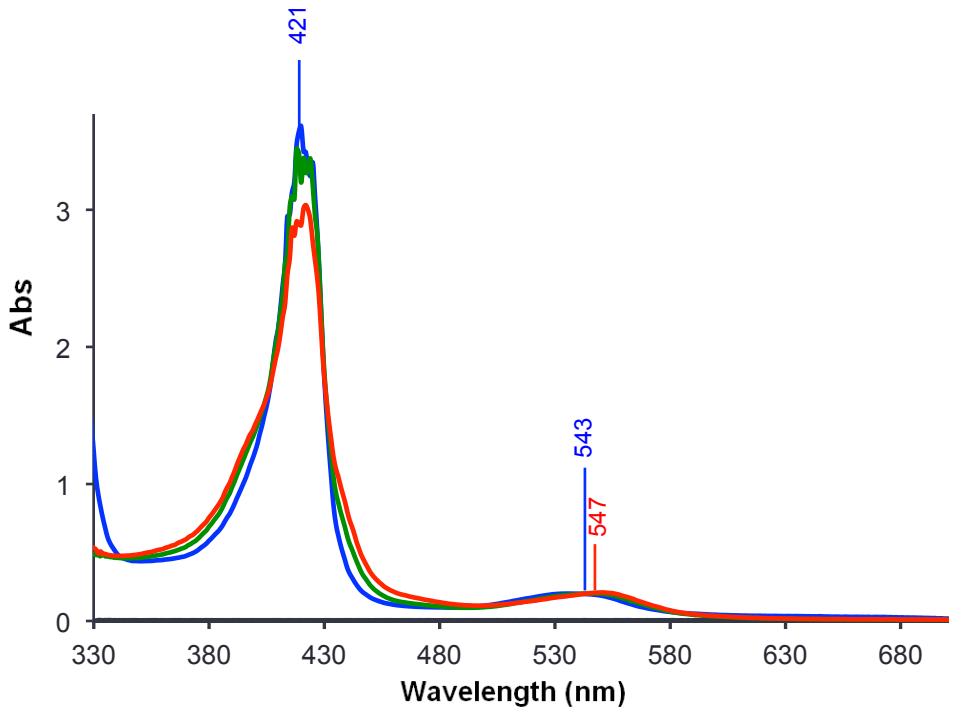

Figure S13. UV-vis spectra of F_8Fe^{II} and $[(tmpa)Cu^{I}(MeCN)][B(C_6F_5)_4]$ (blue, λ_{max} = 421 (Soret), 543 nm) followed by addition of 1 equiv of $(Bu)_4N(NO_2)$ after stirring for 30 min (green) for 3 h (red, λ_{max} = 421 (Soret), 547 nm) (15 μM) in acetone at RT.

12. Reaction of $[F_8Fe^{III}\text{-}O\text{-}Cu^{II}(tmpa)][B(C_6F_5)_4]$ with $NO_{(g)}$

In a 25 mL-Schlenk flask equipped with a magnetic stir bar was added in the drybox $(F_8)Fe^{II}$ (12 mg, 0.015 mmol) and $[(tmpa)Cu^{I}(MeCN)][B(C_6F_5)_4]$ (16 mg, 0.015 mmol). Addition of 10 mL MeTHF resulted in the formation of an intense red solution, which was then bubbled with dry dioxygen to generate $[(F_8)Fe^{III}\text{-}O\text{-}Cu^{II}(tmpa)][B(C_6F_5)_4]$. The mixture was allowed to stir for 1 h and the solvent was removed under vacuum. The solid product was then redissolved in 10 mL deoxygenated acetone and 34 μL of the solution was diluted with acetone to 5.0 mL, and a UV-vis spectrum was recorded. Then 2 mL of $NO_{(g)}$ was bubbled through this solution, and the UV-vis spectrum (**Figure S14**) showed the fast formation of $(F_8)Fe^{II}(NO)$ {λ_{max} = 399 (Soret), 540 nm}. Another UV-vis sample was prepared and only 1 mL of $NO_{(g)}$ was directly bubbled into the solution resulting in a slower disappearance of $[(F_8)Fe^{III}\text{-}O\text{-}Cu^{II}(tmpa)][B(C_6F_5)_4]$ {λ_{max} = 435 (Soret), 555 nm} followed by formation of $(F_8)Fe^{II}(NO)$ {λ_{max} = 399

(Soret), 540 nm} (**Figure S15**). The IR spectrum of the solid sample (ν_{NO} = 1688 cm^{-1}) directly indicates nitrosyl complex, $(F_8)Fe^{II}(NO)$ formation. An EPR spectrum **(Figure S16)** in acetone at 20 K revealed a mixture of Cu^{II} and heme-Fe-NO compounds. A sample (1 mM) of the reaction product of reaction of $(F_8)Fe^{III}$-O-$Cu^{II}(tmpa)][B(C_6F_5)_4]$ and $NO_{(g)}$ in acetone at 20 K was identical in all regards to that of an authentic sample of a 1:1 mixture of $(F_8)Fe^{II}(NO)$ and $[(tmpa)Cu^{II}(NO_2)][B(C_6F_5)_4]$ (1 mM in acetone at 20 K), see **Figure S16**.

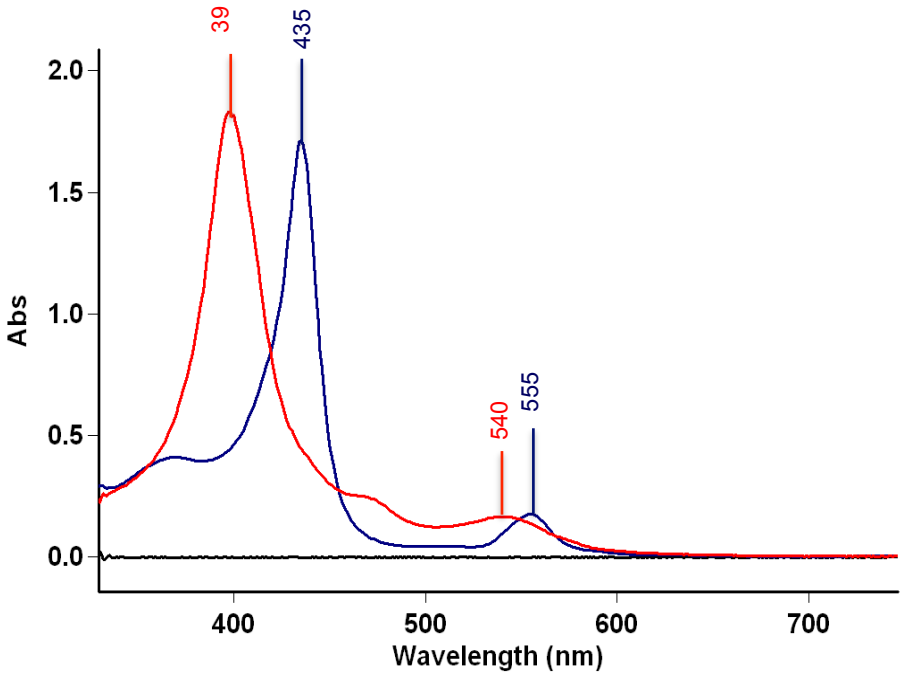

Figure S14. UV-vis spectra of $(F_8)Fe^{III}$-O-$Cu^{II}(tmpa)][B(C_6F_5)_4]$ (**1**)(blue), $(F_8)Fe^{II}(NO)$ (red) generated from **1** + 2 mL of $NO_{(g)}$ (12 μM) in acetone at RT.

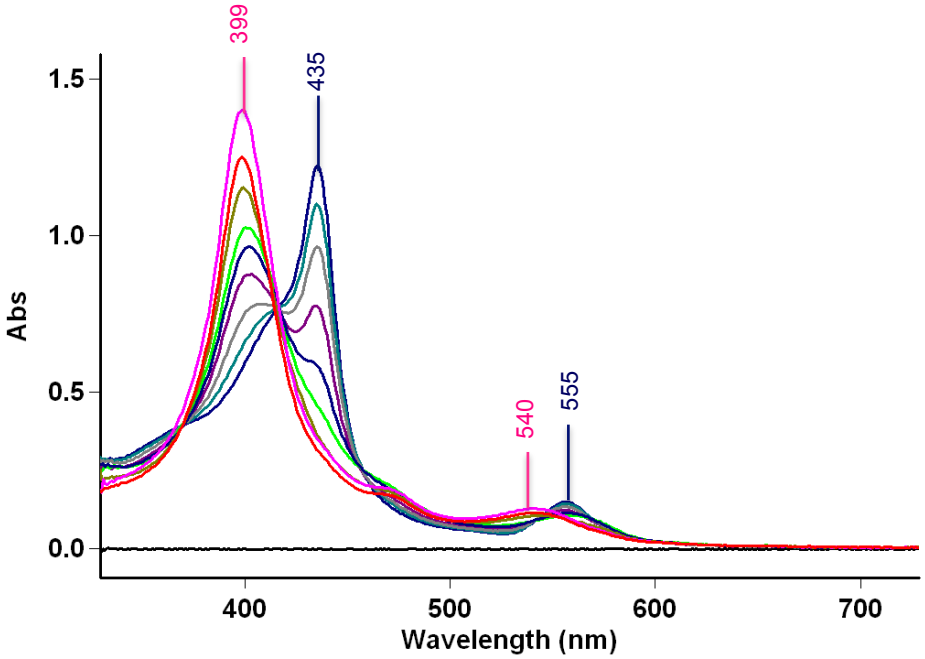

Figure S15. UV-vis spectra of $[(F_8)Fe^{III}\text{-O-}Cu^{II}(tmpa)][B(C_6F_5)_4]$ (**1**) (blue), $(F_8)Fe^{II}(NO)$ (red) generated from **1** + 1 mL of $NO_{(g)}$ (the time intervals between two consecutive spectra (Δt) were approximately 1, 2, 1.5, 1.5, 2, 6, and 16 minutes respectively). Addition of second mL of $NO_{(g)}$ to the solution resulted in completion of the reaction (purple) (10 μM) in acetone at RT.

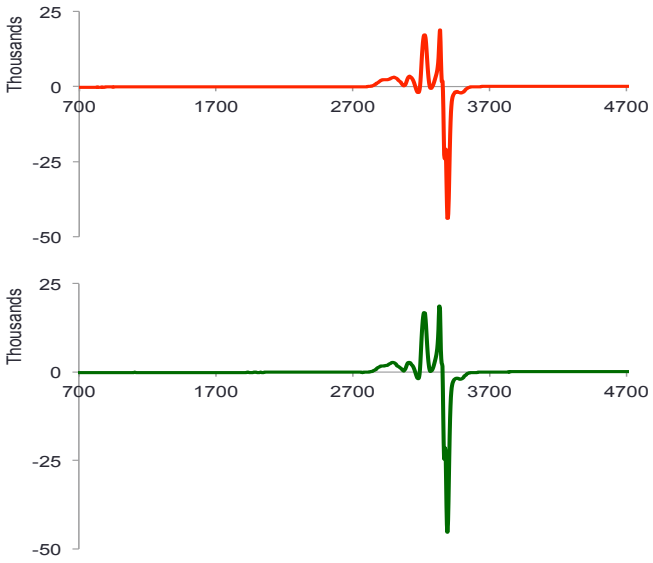

Figure S16. EPR spectrum comparison between the reaction product and an authentic sample: the products of the reaction between $[(F_8)Fe^{III}\text{-O-}Cu^{II}(tmpa)][B(C_6F_5)_4]$ and $NO_{(g)}$, giving signals of $(F_8)Fe^{II}(NO)$ and Cu^{II}(**red**); an authentic sample of a 1:1 mixture of $(F_8)Fe^{II}(NO)$ and $[(tmpa)Cu^{II}(NO_2)][B(C_6F_5)_4]$ (**green**) (1 mM) in MeTHF at 20 K.

13. Titration of the product of reaction of $[F_8Fe^{III}\text{-}O\text{-}Cu^{II}(tmpa)][B(C_6F_5)_4]$ with $NO_{(g)}$

The product mixture, $(F_8)Fe^{II}(NO)$ and $[(tmpa)Cu^{II}(NO_2)]^+$(11.8 mg, 0.006 mmol), derived from reaction of $[F_8Fe^{III}\text{-}O\text{-}Cu^{II}(tmpa)][B(C_6F_5)_4]$ (11.4 mg, 0.006 mmol) with excess $NO_{(g)}$ (see above), was dissolved in 25 mL of deoxygenated acetone inside the drybox. To generate a 10 μM UV-vis sample, a 203 μL aliquot was withdrawn by syringe and diluted with acetone to 5.0 mL and UV-vis spectrum was recorded (λ_{max} = 399 (Soret), 540 nm). Then, $(F_8)Fe^{II}$ (10.0 mg, 0.012 mmol) was added to the product solution and the solution mixture was diluted with acetone to 50 mL and stirred for 30 min. A UV-vis spectrum (**Figure S17**) of the resulting solution revealed the presence of a nearly 2:1 mixture of $(F_8)Fe^{II}(NO)$ (λ_{max} = 399 nm) and $[(F_8)Fe^{III}\text{-}O\text{-}Cu^{II}(tmpa)]^+$ (435 nm, sh).

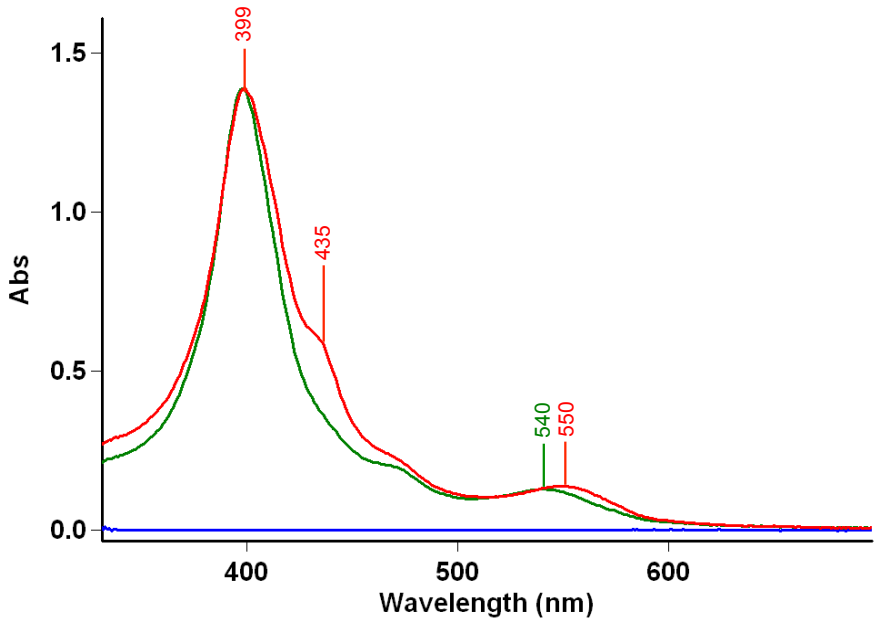

Figure S17. UV-vis spectra of $(F_8)Fe^{II}(NO)$ and $[(tmpa)Cu^{II}(NO_2)][B(C_6F_5)_4]$, derived from the reaction of $[F_8Fe^{III}\text{-}O\text{-}Cu^{II}(tmpa)][B(C_6F_5)_4]$ with excess $NO_{(g)}$ (10 μM) (green, λ_{max} = 399, 540 nm), followed by addition of 2 equiv of F_8Fe^{II} after stirring for 30 min (red, λ_{max} = 399, 435(sh) (Soret), 550 nm) (15 μM based on hemes present in the solution) in acetone at RT.

14. Reaction of $[F_8Fe^{III}\text{-}(OH)\text{-}Cu^{II}(tmpa)][B(C_6F_5)_4]_2$ with $NO_{(g)}$

In the drybox, to a 10 mL MeTHF solution of $[F_8Fe^{III}\text{-}O\text{-}Cu^{II}(tmpa)][B(C_6F_5)_4]$ (32.0 mg, 0.017 mmol), 1 equiv HBArF (14.3 mg, 0.017 mmol) was added. After stirring for 1 h, solvent was removed under reduced pressure, and a brown solid was redissolved in acetone and a UV-vis spectrum revealed the formation of $[F_8Fe^{III}\text{-}(OH)\text{-}Cu^{II}(tmpa)][B(C_6F_5)_4]_2$. Then 3.5 mL of $NO_{(g)}$ was bubbled through this solution; no significant absorbance change was detected in UV-vis spectrum of the resulting solution, see **Figure S18**. After several hours of stirring formation of $(F_8)Fe^{II}(NO)$ was observed due to the well-known reductive nitrosylation reaction. Then, the solvent was removed and the solid product obtained was used for nitrite analysis, however, no nitrite ion was detected (see below for sample preparation for nitrite analysis).

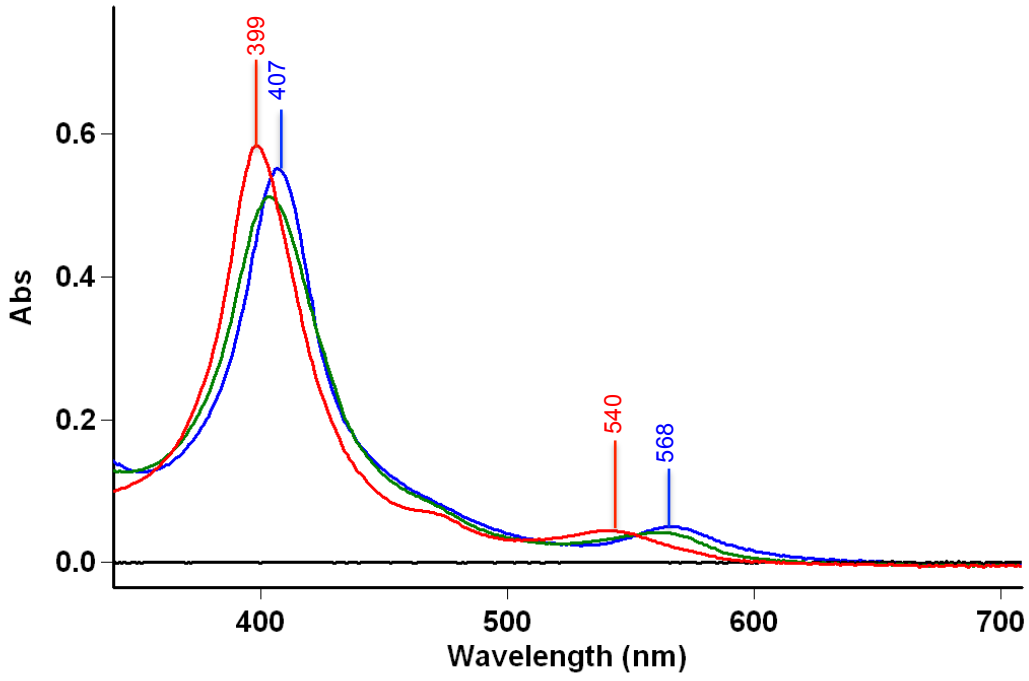

Figure S18. UV-vis spectra of $[F_8Fe^{III}\text{-}(OH)\text{-}Cu^{II}(tmpa)][B(C_6F_5)_4]_2$ (blue, λ_{max} = 407 (Soret), 568 nm) and after bubbling 5 mL $NO_{(g)}$ into the solution and stirring for 20 min (green, λ_{max} = 405 (Soret), 565 nm) after stirring for 5 h generating $(F_8)Fe^{III}(NO)$ (red, λ_{max} = 399 (Soret), 540 nm), 7 μM in acetone at RT.

15. Reaction of $F_8Fe^{III}(OH)$ with $NO_{(g)}$

In a 50 mL-Schlenk flask equipped with a magnetic stir bar, $(F_8)Fe^{II}(OH)$ (30 mg, 0.036 mmol) was dissolved in 25 mL acetone in the drybox. Then 5 mL $NO_{(g)}$ was bubbled through this solution using a three-way syringe. After stirring for several hours, the solvent was removed under reduced pressure and solid product was redissolved in 10 mL CH_2Cl_2 and nitrite analysis of an aqueous solution derived from the reaction mixture indicated no trace of nitrite was present. UV-vis monitoring of the reaction mixture indicated only a very slow (hours) reductive nitrosylation occurred where the heme present was converted to $(F_8)Fe^{II}(NO)$, see **Figure S19**.

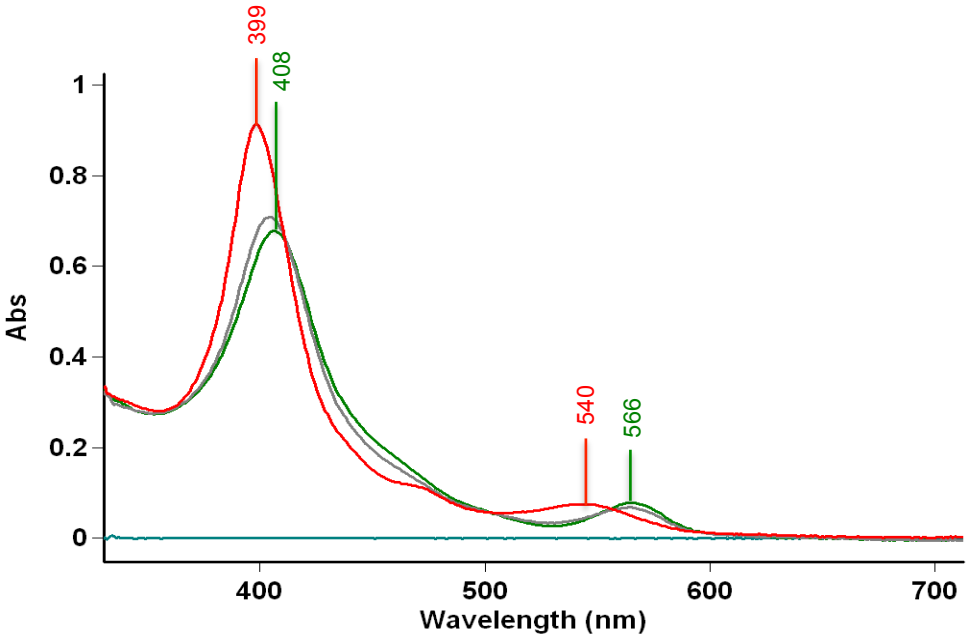

Figure S19. UV-vis spectra of $(F_8)Fe^{III}(OH)$ (green, λ_{max} = 408 (Soret), 566 nm; 8 μM in acetone at RT) and after bubbling 5 mL $NO_{(g)}$ into the solution and stirring for 20 min (gray, λ_{max} = 406 (Soret), 565 nm), after stirring for 5 h generating $(F_8)Fe^{III}(NO)$ (red, λ_{max} = 399 (Soret), 540 nm).

16. Rapid electron transfer from Cu^I to Fe^{III} and redox equilibrium

To a 100 mL Schlenk flask equipped with a magnetic stir bar was added $(F_8)Fe^{III}(SbF_6)$•2THF (14.7 mg, 0.012 mmol) in 50 mL deoxygenated acetone under a N_2 atmosphere. Complex $[(tmpa)Cu^I(MeCN)][B(C_6F_5)_4]$ (13.2 mg, 0.012 mmol) was added to the brown solution inducing an

immediate color change to red owing to the formation reduced heme F_8Fe^{II}. A UV-vis spectrum of the solution mixture (**Figure S20**) right after addition of Cu^{I} complex revealed that the electron transfer from Cu^{I} to Fe^{III} readily occurs in acetone, resulting in complete formation of F_8Fe^{II} as a major heme species in solution. After stirring for 1 h, a UV-vis spectrum of reaction mixture showed the presence of both F_8Fe^{II} (λ_{max} = 419 (Soret)) and $(F_8)Fe^{III}(SbF_6)$ (λ_{max} = 395(sh) (Soret)) as the equilibrium in acetone was reached. This redox equilibrium, which is known to be dependent on solvent interaction, concentration, and temperature have already been reported for similar systems.[14] Since the Cu^{I}-to-Fe^{III} electron-transfer readily occurs in the present ligand-complexes, $[(tmpa)Cu^{I}(MeCN)]^{+}$ and $[(F_8)Fe^{III}]SbF_6$, Cu^{I}-NO^{+} resulting from first nitric oxide molecule attack at the cupric center can be proposed as a possible reaction intermediate. Formation of Cu^{I}-NO^{+} can then be followed by a rapid Cu^{I}-to-Fe^{III} electron transfer generating a Cu^{II}-nitrito complex and ferrous heme, the latter is then trapped by a second NO molecule.

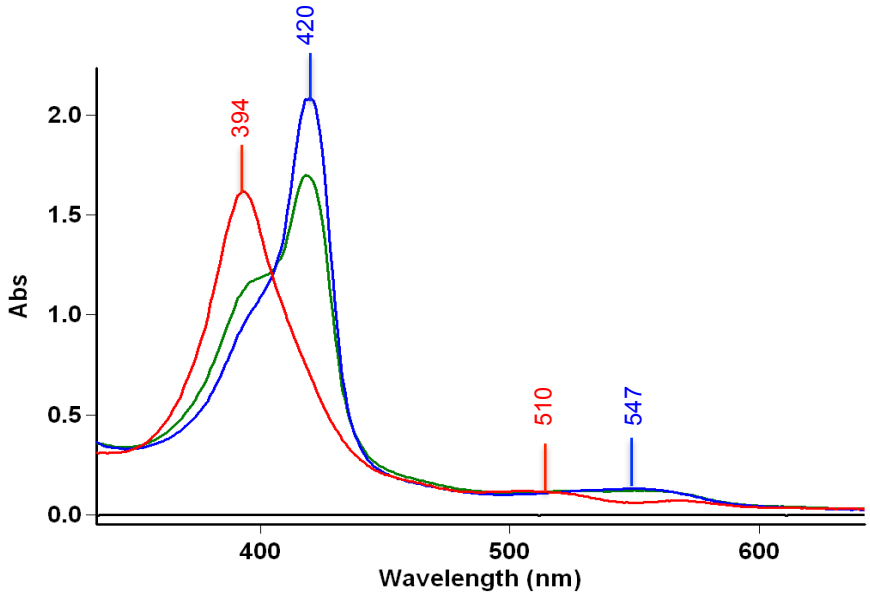

Figure S20. UV-vis spectra of $(F_8)Fe^{III}(SbF_6)$ (red, λ_{max} = 394 (Soret), 510 nm) and solution right after addition of $[(tmpa)Cu^{I}(MeCN)][B(C_6F_5)_4$ (blue, λ_{max} = 420 (Soret), 547 nm) indicating electron transfer from Cu^{I} to Fe^{III} takes place generating $(F_8)Fe^{II}$. After stirring for 30 min, the green spectrum is observed (λ_{max} = 395 (sh), 419 (Soret), 547 nm), representative of an equilibrium state. (The solutions for these experiments are 12 μM based on heme in acetone at RT)

17. Analysis of Nitrite ion by Capillary Electrophoresis

In a 25 mL-Schlenk flask equipped with a magnetic stir bar was added in the drybox $(F_8)Fe^{II}$ (12 mg, 0.015 mmol) and $[(tmpa)Cu^{I}(MeCN)][B(C_6F_5)_4]$ (16 mg, 0.015 mmol). Addition of 10 mL MeTHF resulted in an intense red solution, which was bubbled with dry dioxygen to generate $[(F_8)Fe^{III}\text{-}O\text{-}Cu^{II}(tmpa)][B(C_6F_5)_4]$. The solvent was then removed under vacuum and solid was redissolved in 10 mL deoxygenated acetone followed by direct bubbling of excess NO into the solution via a three-way long syringe needle and stirring for 1h. Then the solvent was removed and solid product was dissolved in 10 mL CH_2Cl_2 and extracted with 25 mL of aqueous NaCl solution (6 mM). The presence of significant amounts of nitrite ion in the aqueous layer was confirmed by semiquantitative QUANTOFIX nitrite test strips as well as the UV-vis spectrum showing a band at 355 nm corresponding to nitrite n —> π^* transitions.[15]

Afterwards, capillary electrophoresis (CE) was used for nitrite quantification in the aqueous layer. A standard calibration curve was first constructed using sodium nitrite. By employing optimal conditions, the calibration curve was generated for a concentration range of 100–2000 μM. This nitrite analysis indicated nitrite (NO_2^-) was present in the product mixture with a yield of 95% (560 μM), according to eq.2.

18. Cyclic Voltammetry Measurements

The Cyclic voltammetry measurements were carried out on $(F_8)Fe^{II}$, $[(tmpa)Cu^{I}(MeCN)][B(C_6F_5)_4]$, $(F_8)Fe^{III}(SbF_6)$•2THF, and $[(tmpa)Cu^{II}(MeCN)](ClO_4)$ complexes under an argon atmosphere in acetone solutions, containing 100 mM $(Bu)_4N(PF_6)$ electrolyte, using 1 and 2 mM complex concentrations for the reduced and oxidized complexes, respectively. The cell consisted of a 50 mL four-necked round bottom flask equipped with rubber septa. Each neck possessed one of the following: a glassy carbon working electrode, an $Ag/AgNO_3$ reference electrode in MeCN, a platinum wire as the auxiliary elec-

trode, and an adapter connected to an argon line. All voltammograms were classified as quasi-reversible having $i_{pc}/i_{pa} \approx 1$ with half-wave potentials in the range $E_{1/2} = -190$ to -425 mV versus Fc^+/Fc. The $E_{1/2}$ values obtained are listed in Table S1. We found that the $E_{1/2}$ values for the copper complexes are more negative than for the heme complexes (Table S1), suggesting that the former is a better reductant.

Table S1. Redox potentials of the heme and copper complexes recorded in acetone at room temperature

Compound	**$E_{1/2}$(mV vs. Fc^+/Fc)** [a]	**ΔE(mV)** [a]	**$E_{1/2}$(mV vs. NHE)** [b]	**Redox Couple**
$(F_8)Fe^{II}$	-190	120	+360	Fe^{III}/Fe^{II}
$(F_8)Fe^{III}(SbF_6)$•2THF	-205	110	+345	Fe^{III}/Fe^{II}
$[(tmpa)Cu^{I}(MeCN)][B(C_6F_5)_4]$	-410	130	+140	Cu^{II}/Cu^{I}
$[(tmpa)Cu^{II}(MeCN)](ClO_4)$	-425	130	+125	Cu^{II}/Cu^{I}

[a] Potentials are reported versus the Fc^+/Fc redox couple and are rounded to the nearest 5 mV.

[b] Potentials are converted to versus NHE by correcting for the expected Fc^+/Fc redox potential of +310 mV versus the KCl-saturated aqueous calomel electrode (SCE), where SCE is +241 mV versus NHE[16] and all values are rounded to the nearest 5 mV.

---

[1] (a) Ford, P. C.; Lorkovic, I. *Chem. Rev.* **2002**, *102*, 993-1017. (b) Wang, J.; Schopfer, M. P.; Sarjeant, A. A. N.; Karlin, K. D. *J. Am. Chem. Soc.* **2009**, 131, 450–451. (c) Schopfer, M. P.; Mondal, B.; Lee, D.-H.; Sarjeant, A. A. N.; Karlin, K. D. *J. Am. Chem. Soc.* **2009**, 131, 11304-11305.

[2] Sheldrick, G.M. *Acta Cryst.* **2008**, A64, 112-122.

[3] Jacobson, R. R.; Tyeklar, Z.; Farooq, A.; Karlin, K. D.; Liu, S.; Zubieta, J. *J. Am. Chem. Soc.* **1988**, 110, 3690-3692.

[4] (a) Fox, S.; Nanthakumar, A.; Wikström, M.; Karlin, K. D.; Blackburn, N. J. *J. Am. Chem. Soc.* **1996**, 118, 24-34. (b) Wang, J.; Schopfer, M. P.; Puiu, S. C.; Sarjeant, A. A. N.; Karlin, K. D. *Inorg. Chem.* **2010**, 49, 1404-1419.

[5] Karlin, K. D.; Nanthakumar, A.; Fox, S.; Murthy, N. N.; Ravi, N.; Huynh, B. H.; Orosz, R. D.; Day, E. P. *J. Am. Chem. Soc.* **1994**, 116, 4753-4763.

[6] Wang, J.; Schopfer, M. P.; Puiu, S. C.; Sarjeant, A. A. N.; Karlin, K. D. *Inorg. Chem.* **2010**, *49*, 1404-1419.

[7] (a) Kopf, M.-A.; Neuhold, Y.-M.; Zuberbühler, A. D.; Karlin, K. D. *Inorg. Chem.* **1999**, 38, 3093-3102. (b) Ghiladi, R. A.; Kretzer, R. M.; Guzei, I.; Rheingold, A. L.; Neuhold, Y. M.; Hatwell, K. R.; Zuberbühler, A. D.; Karlin, K. D. *Inorg. Chem.* **2001,** 40, 5754-5767.

[8] Jutzi, P.; Müller, C.; Stammler, A.; Stammler, H. *Organometallics* **2000**, 19, 1442-1444.

[9] Fox, S.; Nanthakumar, A.; Wikström, M.; Karlin, K. D.; Blackburn, N. J. *J. Am. Chem. Soc.* **1996**, *118*, 24-34.

[10] (a) Zubieta, J.; Karlin, K. D.; Hayes, J. C. "Structural Systematics of Cu(I) and Cu(II) Derivatives of Tripodal Ligands'," In *Copper Coordination Chemistry: Biochemical and Inorganic Perspectives*; K. D. Karlin and J. Zubieta, Ed.; Adenine Press: Albany, New York, **1983**; pp 97-108. (b) Karlin, K. D.; Hayes, J. C.; Juen, S.; Hutchinson, J. P.; Zubieta, J. *Inorg. Chem.* **1982**, 21, 4106-4108.

[11] Addison, A. W.; Rao, T. N.; Reedijk, J.; Van Rijn, J.; Verschoor, G. C. *J. Chem. Soc., Dalton Trans.* **1984**, 1349–1356.

[12] (a) Lucas, H. R.; Meyer, G. J.; Karlin, K. D. *J. Am. Chem. Soc.* **2010**, 132, 12927-12940.

[13] Liang, H. C.; Kim, E.; Incarvito, C. D.; Rheingold, A. L.; Karlin, K. D. *Inorg. Chem.* **2002**, 41, 2209-2212.

[14] Fry, H. C.; Lucas, H. R.; Zakharov, L. N.; Rheingold, A. L.; Meyer,G. J.; Karlin, K. D. *Inorg. Chim. Acta* **2008**, 361, 1100-1115.

[15] Jankowski, J. J.; Kieber, D. J.; Mopper, K. *Photochem. Photobiol.* **1999**, 70, 319-328.

[16] Brad, A. J.; Faulkner, L. R. *Electrochemical Methods: Fundamentals and applications*, 2nd Ed.; Wiley: New York, **2001**.